ACS APPLIED MATERIALS & INTERFACES

Research Article

www.acsami.org

Hierarchical Micron-Sized Mesoporous/Macroporous Graphene with Well-Tuned Surface Oxygen Chemistry for High Capacity and Cycling Stability Li–O_2 Battery

Wei Zhou,[†,‡] Hongzhang Zhang,[†] Hongjiao Nie,[†,‡] Yiwen Ma,[†] Yining Zhang,*[,†] and Huamin Zhang*[,†]

[†]Division of Energy Storage, Dalian National Laboratory for Clean Energy, Dalian Institute of Chemical Physics, Chinese Academy of Sciences, Zhongshan Road 457, Dalian 116023, China

[‡]University of Chinese Academy of Sciences, Beijing 100039, China

Supporting Information

ABSTRACT: Nonaqueous Li–O_2 battery is recognized as one of the most promising energy storage devices for electric vehicles due to its super-high energy density. At present, carbon or catalyst-supporting carbon materials are widely used for cathode materials of Li–O_2 battery. However, the unique electrode reaction and complex side reactions lead to numerous hurdles that have to be overcome. The pore blocking caused by the solid products and the byproducts generated from the side reactions severely limit the capacity performance and cycling stability. Thus, there is a great need to develop carbon materials with optimized pore structure and tunable surface chemistry to meet the special requirement of Li–O_2 battery. Here, we propose a strategy of vacuum-promoted thermal expansion to fabricate one micron-sized graphene matrix with a hierarchical meso-/macroporous structure, combining with a following deoxygenation treatment to adjust the surface chemistry by reducing the amount of oxygen and selectively removing partial unstable groups. The as-made graphene demonstrates dramatically tailored pore characteristics and a well-tuned surface chemical environment. When applied in Li–O_2 battery as cathode, it exhibits an outstanding capacity up to 19 800 mA h g^{-1} and is capable of enduring over 50 cycles with a curtaining capacity of 1000 mA h g^{-1} at a current density of 1000 mA g^{-1}. This will provide a novel pathway for the design of cathodes for Li–O_2 battery.

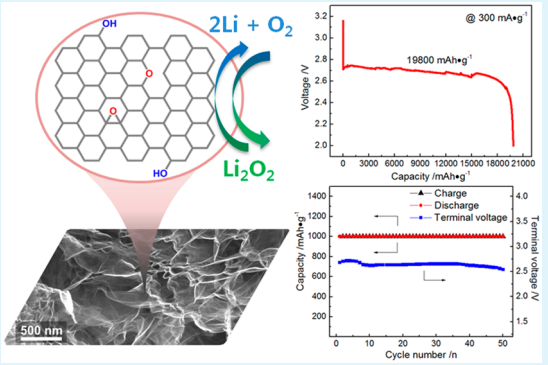

KEYWORDS: *Li–O_2 battery, graphene, hierarchical structure, oxygen functional group, oxygen electrode*

1. INTRODUCTION

Nonaqueous Li–O_2 battery has been considered as a candidate power source for electrical vehicles due to its extremely high theoretical energy density that is comparable to gasoline.[1−3] The main factors restraining the application of nonaqueous Li–O_2 battery are the stability of electrolyte[3−8] and the design of oxygen cathode.[9−15] Conventional electrolyte, such as carbonate-based or ether-based electrolyte, is easily decomposed in the highly oxidizing environment,[5,6] and cannot efficiently support the operation of Li–O_2 battery. Recently, dimethyl sulfoxide (DMSO) was proved to be compatible with discharge product-Li_2O_2 by Bruce et al.,[16,17] although some indications of side reaction were observed when operating with carbon electrode.[8] However, even if we have established an ultimately stable electrolyte system, the design of cathode still remains a critical challenge for the application of Li–O_2 battery.

The oxygen cathode, which is widely used carbon or catalyst-supporting carbon, provides the space and surface for oxygen reduction reaction (ORR) and oxygen evolution reaction (OER). During discharge, the insoluble Li_2O_2 product locates on the surface of cathode material and is stored in the pores (ORR process), followed by its decomposition to Li^+ and O_2 during charge (OER process). As the solid-state Li_2O_2 continuously deposits at oxygen electrode, it gradually blocks the transport of oxygen and lithium ion and will prevent further reaction. That means the electrically isolated product will passivate cathode surface, thus leading to limited rate capability and capacity fading.[3,11,18−21] Therefore, a well-designed architecture with sufficient reactants diffusion channels and large pore volume for the storage of solid product will be beneficial. For this consideration, numerous carbon cathodes with desired structure have been applied in Li–O_2 battery, such as mesoporous carbon,[22−24] carbon nanotube,[25] carbon fiber,[26] and graphene,[10,27] by the control of structure and porosity.[28,29]

In addition, the sluggish kinetic of the electrochemical reaction will give rise to large voltage gap between discharge and charge, and the byproducts (e.g., Li_2CO_3) generated from the side reactions between Li_2O_2 and carbon will induce poor

Received: December 3, 2014
Accepted: January 16, 2015
Published: January 16, 2015

DOI: 10.1021/am508513m
ACS Appl. Mater. Interfaces 2015, 7, 3389−3397

cycle performance.[7,8,30] To resolve the problem, tremendous researches aim to develop catalyst, such as metal (Co,[31] Pt,[13] Ru,[32] PdCu,[33] etc.) or metal oxide (Co_3O_4,[34] Mn_3O_4,[12] RuO_2,[35] etc.), that is incorporated into carbon materials to decrease the polarization. However, the carbon surface is always dominated in cathode due to its much higher surface area compared to catalyst, and that means catalyst cannot completely cover the entire carbon surface. Unfortunately, the electrochemical reaction will take place on all the carbon surface with or without catalyst covering. It is inevitable that the carbon surface will react with Li_2O_2 during the discharge and charge processes.[7,8,36,37] Because the byproducts are hardly decomposed on charge, the accumulation of byproducts in cathode will lead to continuous passivation of electrochemical reaction interface. This has been regarded as the critical obstacle for the practical employment of carbon materials in Li−O_2 battery.

On the basis of the above analysis, the optimal carbon material for Li−O_2 battery should afford large pore volume to store the discharge product and optimized pore structure to transport lithium ion and oxygen. Besides, the surface of the carbon material should provide a stable electrode/electrolyte interface that could efficiently suppress the side reactions between carbon and Li_2O_2. Herein, we propose a general strategy to prepare a micron-sized porous matrix with hierarchical three-dimensional architectures together with well-tuned surface chemical environment. Graphene, a monolayer of two-dimensional carbon crystal with high surface area, excellent electronic conductivity, variable surface chemistry and easy processing, has been chosen as the building unit to construct the porous matrix. However, when deriving graphene from graphite oxide with a conventional chemical reduction method, for instance, using hydrazine, the strong van der Waals forces between graphene layers always induces irreversible face-to-face restacking,[38−41] which will constrain the development of porosity in the final product. To improve the porosity, we employed a vacuum-promoted, thermal expansion approach to establish the hierarchical structured micron-sized graphene matrix. Subsequently, one deoxygenation process was carried out to adjust the surface chemistry by reducing the amount of surface oxygen and selective removal of some unstable oxygen groups. The as-made graphene demonstrates fertile mesopores and macropores together with a highly reduced graphene surface, which shows synergistic effect on the battery performance: sufficient reaction sites for electrochemical reaction, efficient transportation of lithium ion and oxygen, and slighter side reaction between graphene surface and Li_2O_2. As a result, the Li−O_2 battery fabricated with this graphene cathode delivers an outstanding capacity and exhibits greatly improved cycling stability.

2. EXPERIMENTAL SECTION

2.1. Preparation of Materials. *2.1.1. Preparation of Graphite Oxide.* Graphite oxide was synthesized by an improved Hummers method.[42] First, 3.0 g of graphite and 18.0 g of $KMnO_4$, and 360 mL of concentrated H_2SO_4 and 40 mL of concentrated H_3PO_4 were mixed in advance, respectively. Then, the solid reactants and liquid reactants were added into a 1000 mL baker. The beaker was transferred into the oil bath, and the mixture was stirred for 12 h under 50 °C. The liquid product was poured onto ice (800 mL) with 30% H_2O_2 (15 mL) and formed a yellow solution. Then, the solution was centrifuged, washed by hydrochloric acid (2 times), and washed by deionized water (4 times). The remaining product was dialyzed for 3 days and centrifuged to remove solid impurities. The residual gel product was dried at 30 °C to obtain graphite oxide solid.

2.1.2. Preparation of CRG. Hydrazine was selected as the reductant for the chemical conversion of graphite oxide to graphene. The graphite oxide was added into water and ultrasound dispersed for 8 h. The homogeneous dispersion (50 mL) was mixed with 10 mL of hydrazine solution (35 wt %) under stirring, and the weight ratio of graphite oxide and hydrazine was about 10:7.[43] Then, the solution was transferred into the oil bath and stirred for 1 h under 95 °C. After being filtered and washed, the chemical reduced graphene was obtained, and it is noted as CRG.

2.1.3. Preparation of VTEG. The expansion of graphite oxide was carried out according to a modified vacuum-promoted exfoliation method.[44] The as-prepared graphite oxide (1 g) was put into an autoclave (100 mL) that was connected to a high-vacuum pump by a steel tube. After the barometer on the steel tube line pointed to −1 bar, the autoclave was introduced into a muffle furnace under 900 °C for 2 min. During the exfoliation process, the high-vacuum pump was still operating. Then, the vacuum-promoted, thermal-expanded graphene was obtained, and it is noted as VTEG.

2.1.4. Preparation of VTEG-HT. The as-prepared VTEG was heated from room temperature to 900 °C at 5 °C min^{-1} and held for 6 h in argon atmosphere. The resulting graphene is noted as VTEG-HT.

2.2. Physical Characterization. X-ray diffraction (XRD) was recorded on a DX-2700 X-ray diffractometer, and the scanning electron microscopy (SEM) was conducted on QUANTA 200F (FEI) at an acceleration voltage of 20 kV. X-ray photoelectron spectroscopy (XPS) was carried out on a surface analysis system (ESCALAB250) equipped with monochromatic Al Kα radiation. All of the XPS spectra were peak fit and analyzed using XPS Peak4.1, and the spectra were calibrated according to the C 1s peak (284.6 eV). N_2 adsorption/desorption was tested at 77 K using an ASAP 2020 system. Brunauer−Emmett−Teller (BET) method was applied to determine the surface area. Pore volumes and the pore size distribution (PSD) curves were calculated from the desorption branches using the Barrett−Joyner−Halenda (BJH) model. Transmission electron microscopy (TEM) was detected by Tecnai G^2 Spirit (FEI) at an acceleration voltage of 120 kV. Thermogravimetric analysis (TGA) was carried out on Thermogravimetric/Differential Thermal Analyzer (Pyris Diamond TG/DTA) with a heating rate of 5 °C min^{-1} from 50 to 900 °C in N_2 flow.

2.3. Electrochemical Characterization. *2.3.1. Preparation of Cathode.* The cathode was prepared by mixing graphene (10 mg) with PTFE solution (5 wt %, 50 mg) in propylene glycol (5 mL) by means of ultrasonic dispersion. The resulting slurry was coated on the carbon paper (16 mm in diameter) with a loading of 0.5 mg per electrode. The coated electrode was dried for 24 h at 80 °C under vacuum to remove residual solvent.

2.3.2. Preparation of Single Cell. The electrochemical cells used to investigate discharge/charge performance were based on a modified swagelok design. The single cell was assembled with the graphene cathode, a lithium anode (16 mm in diameter, 40 μm in thickness) and a glass filter (Whatman) in a glovebox (H_2O < 1 ppm, O_2 < 1 ppm). The electrolyte used here was 0.1 M $LiClO_4$ in dimethyl sulfoxide. A stainless spring was used to ensure good contact of every cell parts. Except for the oxygen inlet and outlet, the cell was completely sealed.

2.3.3. Electrochemical Characterization. The discharge/charge performance was recorded by LAND 2100 system (Wuhan, China). For capacity performance, the applied current density was 300 mA g^{-1} (0.075 mA cm^{-2}), and the cutoff voltage was 2.0 V. For cycling performance, the current density was 1000 mA g^{-1} (0.25 mA cm^{-2}). The electrochemical impedance spectroscopy (EIS) was measured at the beginning of discharge with a Solarton 1287 test system in a frequency range of 10^5−10^{-1} Hz. Before each electrochemical characterization, the cell was exposed to the flow oxygen for 2 h.

3. RESULTS AND DISCUSSION

The preparation process of VTEG is shown in Scheme 1. The left side is the precursor-graphite oxide that is highly compacted

DOI: 10.1021/am508513m
ACS Appl. Mater. Interfaces 2015, 7, 3389−3397

Scheme 1. Schematic Illustration of the Preparation Process of VTEG

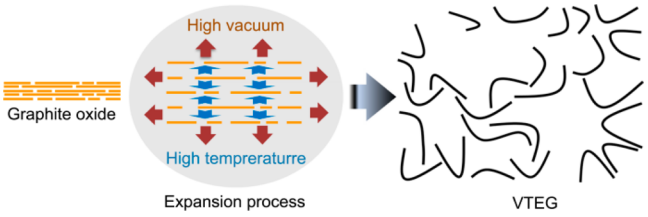

(Figure 1b) and is decorated by large amounts of oxygen functional groups (Figure S1, Supporting Information), such as

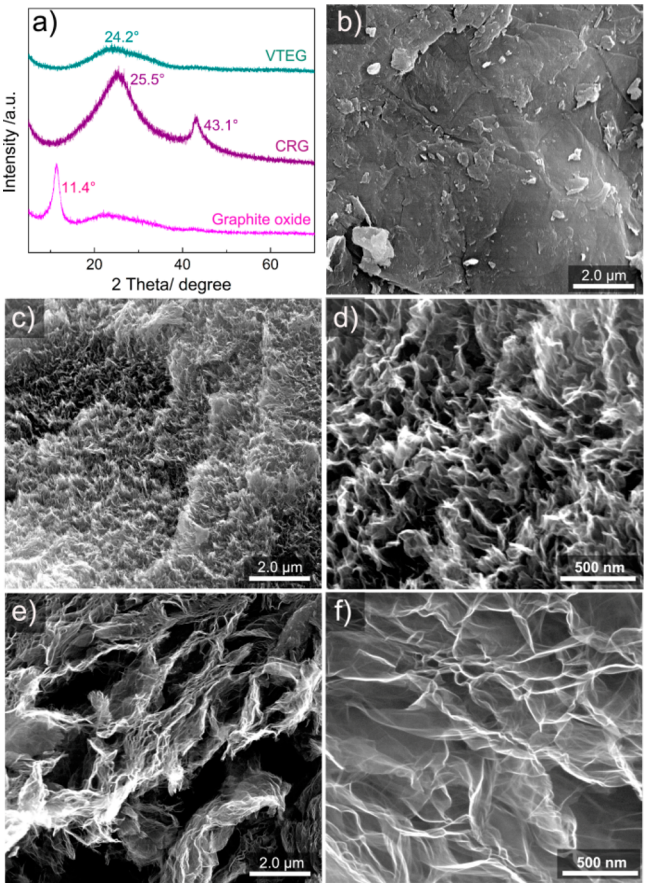

Figure 1. (a) XRD patterns of graphite oxide, CRG, and VTEG; SEM images of (b) graphite oxide, (c and d) CRG, and (e and f) VTEG.

COOH, C═O, C−O and O−H. When expansion is processing, the pyrolytic gas generated from the decomposition of oxygen groups will give rise to high inner stress. And on a high vacuum condition, the inner stress is reinforced to help expand the interspace of graphite oxide layers into nanosized pores and micron-sized pores.

XRD was conducted to confirm the transformation of graphite oxide to graphene. As shown in Figure 1a, the peak at 11.4° which is the characteristic peak of graphite oxide shifts to 24.2° after expansion, indicating the formation of graphene. By comparison, the diffraction peaks on chemical reduced graphene (CRG) pattern are sharper and narrower than that of VTEG and one extra peak at 43.1° is detected, suggesting the agglomeration in CRG is serious.

We further investigated the aggregation state of CRG and VTEG using electron microscopic observations. Although the individual sheets show similar crumpled texture based on transmission electron microscopy observations (Figure S2, Supporting Information), the architectures fabricated by the graphene sheets exhibit visible distinction (Figure 1c−f). Due to the strong interlayer van der Waals attractions, the CRG sheets stack closely to form a dense morphology. While, with high inner stress of the pyrolytic gas to overcome the interlayer attractions, the VTEG sheets were expanded to assemble a micron-sized, highly porous, hierarchically three-dimensional framework. The continuous pores distribute randomly in the graphene matrix with size ranging from micron-size to nanosize. It should be noted that these pores are interconnected from the inside to the outside due to the nature of this expansion method. These pores act as path ways for the pyrolytic gas during the thermal expansion process, and in turn, they function as the oxygen and lithium ion diffusion channels when applied in Li−O_2 battery. The nanosized pores that provide reaction sites were quantificationally measured by nitrogen adsorption−desorption isotherms (Figure S3, Supporting Information) and the corresponding pore size distribution curves are shown in Figure 4. The pore size distribution of CRG totally concentrates at 3−4 nm. In contrast, the VTEG exhibits broad pore size distribution from 2 to 200 nm and the meso-/macropore volume is far greater than CRG (1.74 cm^3 g^{-1} vs 0.01 cm^3 g^{-1}; Table S1, Supporting Information), additionally, the surface area of meso-/macropores is 192.1 m^2 g^{-1} versus 17.1 m^2 g^{-1} (Table S1, Supporting Information). Therefore, with numerous reaction sites and efficient transportation of reactants, the unique pore structure of VTEG is expected to be an ideal design for oxygen cathode.

Figure 2a demonstrates the discharge performance of Li−O_2 battery utilizing oxygen electrode prepared with CRG and VTEG. The capacity of VTEG cathode reaches 13 700 mA h g^{-1}. In contrast, CRG cathode only delivers 1780 mA h g^{-1}. And the discharge voltage plateau of VTEG is 60 mV higher than that of CRG cathode (2.76 V vs 2.70 V). The increased capacity and voltage plateau confirms that the battery performance is greatly beneficial from the hierarchical structure of VTEG. And the cycling stability of the two cathodes was investigated by controlling discharge−charge depth (1000 mA h g^{-1}) at a current density of 1000 mA g^{-1}. Because CRG cathode only delivers 400 mAh g^{-1} at this current density (Figure S4, Supporting Information), its cycling stability did not proceed further. However, the VTEG cathode also exhibits poor cycling performance. As shown in Figure 2b, the discharge terminal voltage of VTEG cathode rapidly decays to 2.0 V after only 2 cycles, and the discharge capacity is about 800 mAh g^{-1}, except the first cycle. As mentioned above, the cycle life of Li−O_2 battery is closely associated with the byproducts generated from the reaction between the carbon surface and Li_2O_2. Thus, in order to improve the cycling stability of VTEG cathode, the surface properties need to be further tuned.

As inherited from the precursor graphite oxide, VTEG sheets are also decorated by diverse functional groups. It is believed that hydroxyl and epoxide groups are bounded on the basal plane and carbonyl, carboxyl are located at the edges of graphene sheets.[45] These oxygen groups predominately determined the surface chemistry of graphene, which will influence the reactivity between carbon and other chemicals, as well as the nucleation of product on carbon substrate. To tune the surface properties of VTEG, we selected a deoxygenation

DOI: 10.1021/am508513m
ACS Appl. Mater. Interfaces 2015, 7, 3389−3397

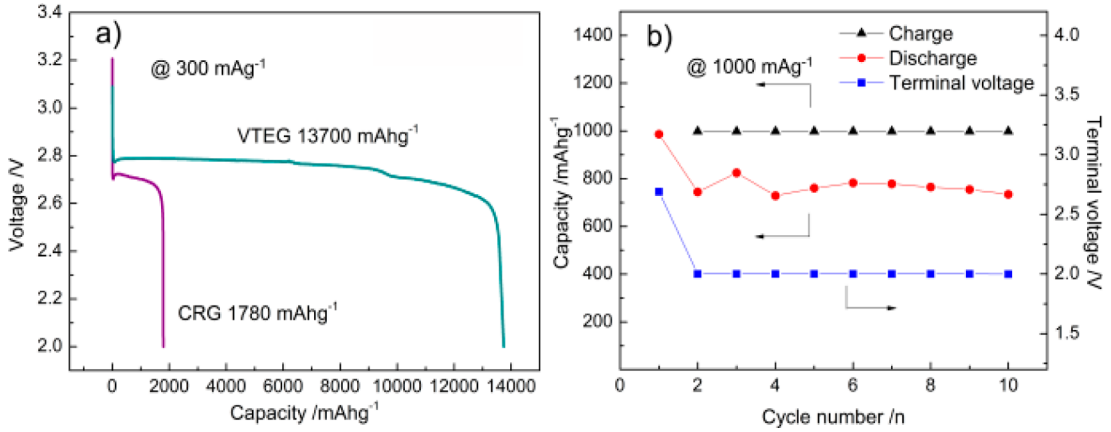

Figure 2. (a) Initial discharge curves for Li−O_2 battery fabricated with CRG cathode and VTEG cathode and (b) cycling profile for Li−O_2 fabricated with VTEG cathode.

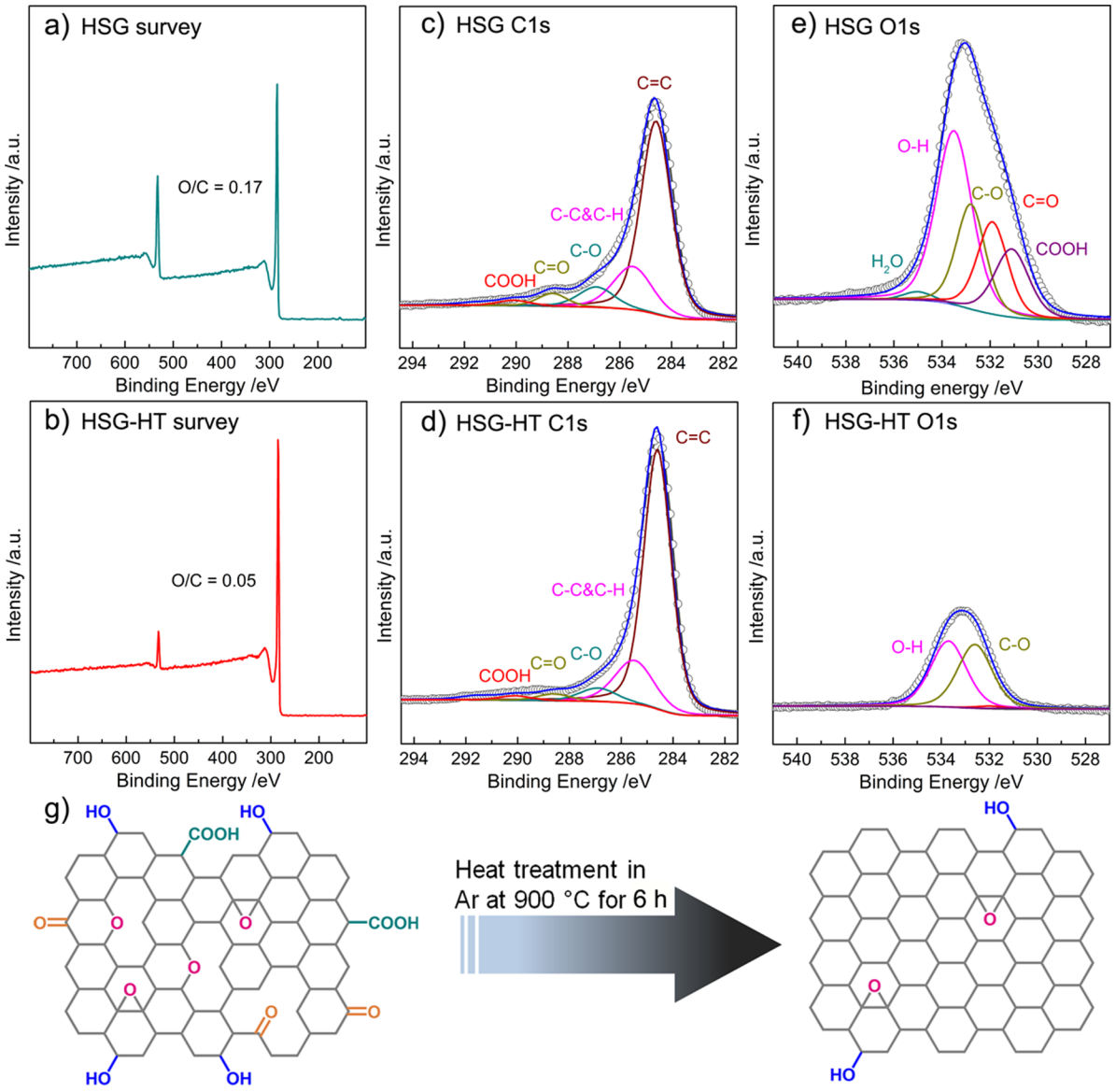

Figure 3. (a and b) XPS survey, (c and d) C 1s spectra, and (e and f) O 1s spectra for (a, c, and e) VTEG and (b, d, and f) VTEG-HT. (g) Schematic illustration of oxygen functional groups on (left) VTEG and (right).

DOI: 10.1021/am508513m
ACS Appl. Mater. Interfaces 2015, 7, 3389−3397

strategy of heat treatment to reduce the abundance of oxygen and selectively eliminate some unstable groups. After the sample was annealed for 6 h at 900 °C in the tube furnace under argon atmosphere, the O/C atomic ratio significantly decreases to 0.05 of VTEG-HT (the VTEG sample after heat treatment is noted as VTEG-HT) from 0.17 of VTEG, as shown in Figure 3a,b, indicating that a majority of oxygen functional groups are removed from VTEG surface.

The evolution of surface oxygen functional groups was further investigated by the C 1s and O 1s fine scan spectra. As shown in Figure 3c,d, the intensity of C═C (284.6 eV) component obviously increases after heat treatment. Meanwhile, the abundance of C−O (286.9 eV[46]) species is correspondingly reduced, suggesting that some oxygen heteroatoms are removed from VTEG surface during the annealing process. Moreover, the intensity of C═O (288.6 eV[46]) and COOH (290.1 eV[46]) on VTEG-HT surface is quite low, indicating a lower content of these functional groups. Results provided by fitting O 1s spectra are more reliable to highlight the change in the types of oxygen functional groups. The pristine VTEG surface distributes plentiful groups of O−H, C−O, C═O, and COOH. After heat treatment, O−H (533.6 eV[47]) and C−O (532.8 eV[48]) become the predominant groups. In contrast, it is hard to detect C═O (531.9 eV[48]) and COOH (531.2 eV[48]) on VTEG-HT surface, suggesting selective removal of C═O and COOH groups. This may be ascribed to their relatively low thermal stability or the conversion of C═O and COOH to other chemical species.[49,50] Besides, the content of C═O and COOH is less than that of C−O and O−H, and thus, it is possible that they may decompose completely earlier than C−O and O−H groups. In brief, the reduction of the amount of oxygen and the elimination of unstable groups leave a largely reduced form of graphene that is expected to be a better candidate for Li−O_2 battery.

Unexpectedly, the meso-/macropore property of VTEG is simultaneously modified with the reduction of oxygen groups. As shown in Figure 4, the PSD curve of VTEG-HT shows much higher pore volume than that of VTEG. Actually, the meso-/macropore volume of VTEG-HT increases from 1.74 $cm^3\ g^{-1}$ of VTEG to 2.84 $cm^3\ g^{-1}$ (a 63% increase; Table S1, Supporting Information), and the surface area of meso-/macropores increases from 192.1 $m^2\ g^{-1}$ to 283.6 $m^2\ g^{-1}$ (a 48% increase; Table S1, Supporting Information), which would provide more reaction sites for electrochemical reaction. The improvement of meso-/macropore properties may be attributed to the conjunction of interlayers broken by the removal of oxygen groups.[51] In addition, the weight-loss of VTEG during heat treatment is relatively high (Figure S5, Supporting Information), suggesting the reaction between graphene and pyrolytic gas (CO_2 and H_2O). And this would also help to construct the meso-/macropores. More importantly, since the temperature was restricted to be less than 1000 °C, no structure shrinking phenomenon of the hierarchical structure is observed.[52] The VTEG-HT material has retained the original open framework (Figure S6, Supporting Information), which ensures facile accessibility of lithium ion and oxygen to the inner part of graphene matrix.

Figure 5a,b demonstrates the capacity performance and cycling stability of Li−O_2 battery fabricated with VTEG-HT cathode. Interestingly, the battery delivers an outstanding capacity as high as 19 800 mA h g^{-1}. And it is worth noting that the capacity could still remain a high value of 1100 mA h g^{-1},

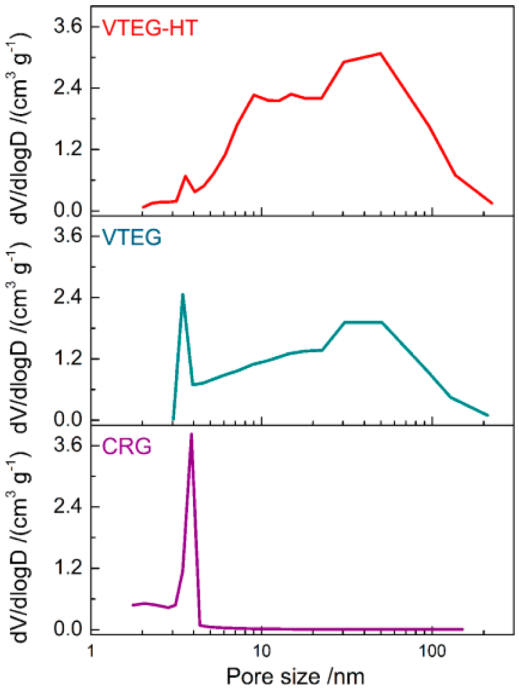

Figure 4. Pore size distributions of CRG, VTEG, and VTEG-HT.

based on the total weight of carbon and discharge product, Li_2O_2, which is nearly 94.4% of the theoretical value (1165 mA h g^{-1} for pure Li_2O_2). Subsequently, the cycling stability of VTEG-HT cathode was evaluated at 1000 mA g^{-1} by controlling the charge−discharge depth of 1000 mA h g^{-1}. The VTEG-HT cathode shows greatly enhanced cycling stability. Remarkably stable cycles were achieved, which could continue over 50 cycles. And the discharge terminal voltage still remains above 2.0 V at the end of cycle test. This is far superior to the VTEG cathode. The enhanced cycling behavior of VTEG-HT is further confirmed by the initial five discharge/charge curves. The voltage gap for VTEG cathode increases rapidly from 1.55 to 2.05 V. While in the case of VTEG-HT cathode, the discharge/charge profiles do not change significantly, and the voltage gap between charge and discharge remains at nearly 1.51 V, indicating that the cycling performance is further improved by varying surface oxygen functional groups.

The large discharge capacity is attributed to three aspects. First, the increased meso-/macropores provide more reaction space and sites for oxygen reduction. The impedance spectra fitted by a typical equivalent circuit for Li−O_2 battery[22,53,54] are shown in Figure S7 (Supporting Information), and the obtained data are given in Table S2 (Supporting Information) clearly demonstrate that the interfacial resistance (R_{int}) and the charge transfer resistance (R_{ct}) of VTEG-HT are smaller than that of VTEG. Second, the open porous framework enhances the diffusion of lithium ion and oxygen from outside to the inside of graphene, which supports enough reactants for the electrochemical reaction. Additionally, a smaller amount of byproducts generated on VTEG-HT electrode which will be discussed below also benefits the capacity performance.

Considering that the byproducts have great impact on the cycling stability of Li−O_2 battery, XPS was conducted to analyze the surface composition of cathode after discharge. As revealed in the C 1s spectra in Figure 6, the peak of Li_2CO_3 at 289.7 eV[55] representing the byproducts is observed on both

DOI: 10.1021/am508513m
ACS Appl. Mater. Interfaces 2015, 7, 3389−3397

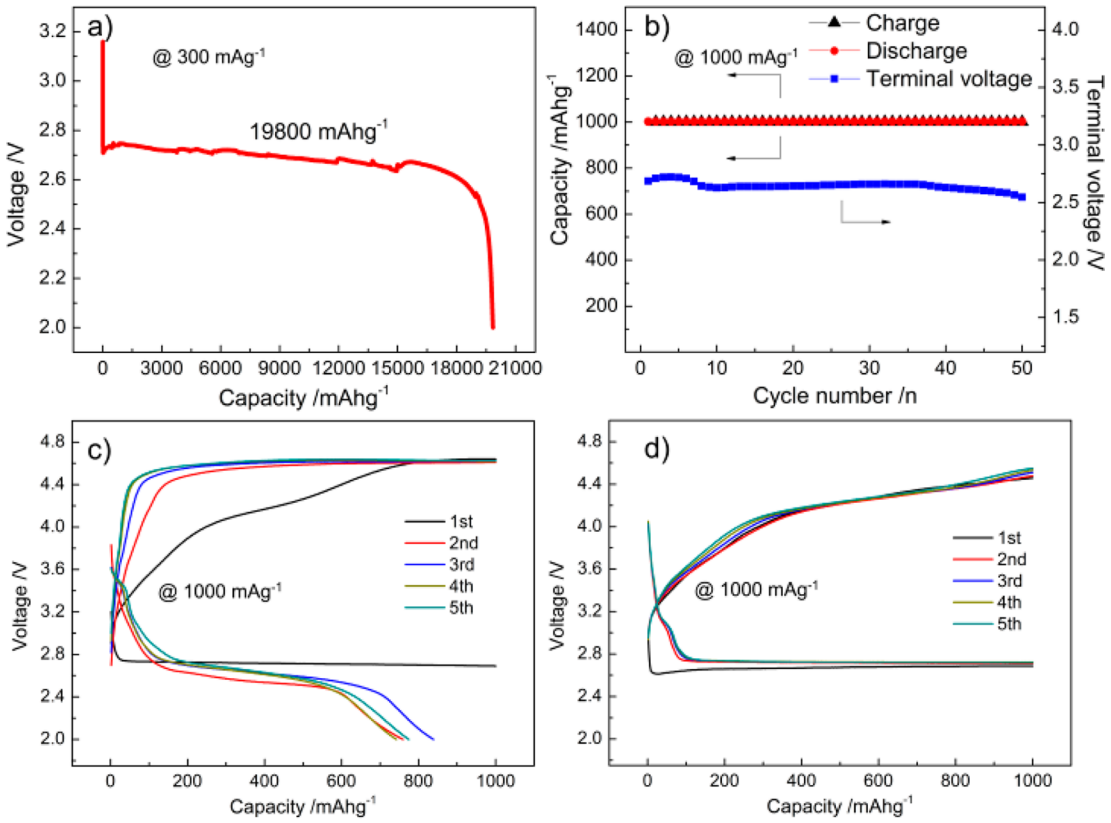

Figure 5. (a) Initial discharge curve for Li−O_2 battery fabricated with VTEG-HT cathode and (b) the cycling profile. Discharge/charge profile of the first five cycles for Li−O_2 battery fabricated with (c) VTEG cathode and (d) VTEG-HT cathode.

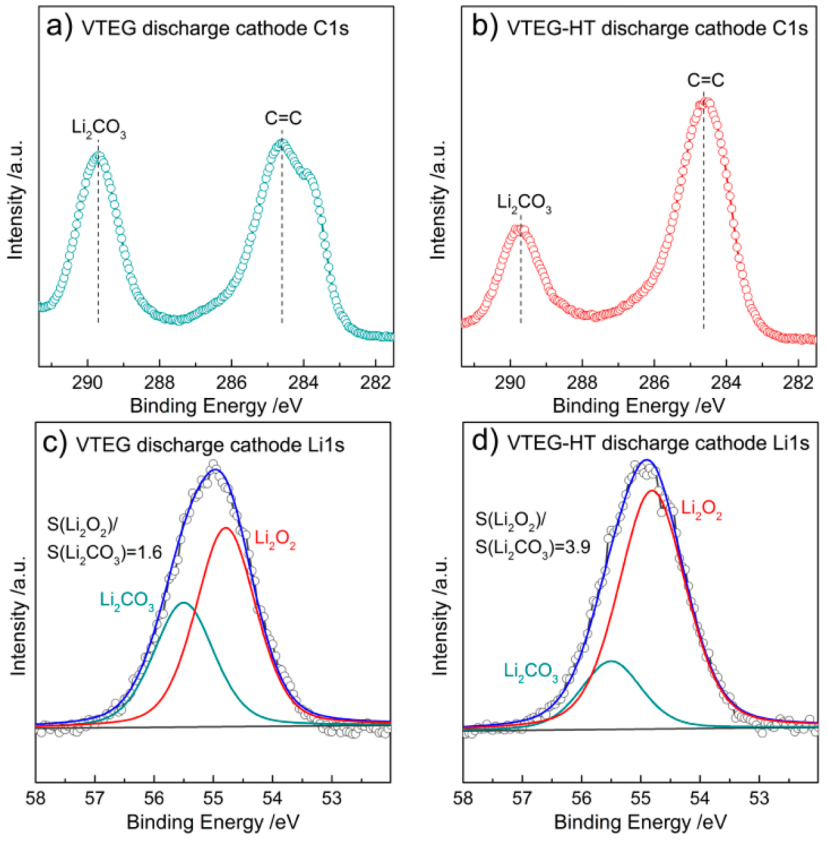

Figure 6. XPS spectra of discharged cathode: C 1s spectra for (a) VTEG cathode and (b) VTEG-HT cathode, Li 1s spectra for (c) VTEG cathode and (d) VTEG-HT cathode.

DOI: 10.1021/am508513m
ACS Appl. Mater. Interfaces 2015, 7, 3389−3397

cathode surface in addition to the C=C peak corresponding to the basic graphene. The lower emission intensity of Li_2CO_3 in VTEG-HT cathode indicates the amount of byproducts on VTEG-HT cathode surface is smaller than VTEG cathode, which is further confirmed by the Li 1s spectra. When switching to Li 1s spectra, Li_2O_2 (54.8 eV[56]) and Li_2CO_3 (55.5 eV[56]) can be found on both graphene surfaces, while VTEG-HT cathode contains predominated proportion of Li_2O_2. The area ratio of Li_2O_2/Li_2CO_3 is 3.9 for VTEG-HT cathode and 1.6 for VTEG cathode. As reported, the Li_2CO_3 layer will cause the drop of exchange current density leading to high polarization[7] and it is hardly to be decomposed during charge, resulting in rapidly increased polarization at the following cycles. Therefore, with a smaller amount of byproducts generated on VTEG-HT surface, the VTEG-HT cathode exhibits greatly enhanced cycling stability.

To explain the formation of Li_2CO_3 on graphene surface, we propose the following hypothesis. Due to the stronger electronegativity of oxygen compared with carbon (3.04 vs 2.04), carbon becomes relatively electropositive when it forms a covalent bond with oxygen, such as COOH, C=O, C−O. And the intermediate product O^{2-} and discharge product Li_2O_2 are powerful nucleophiles[57] in aprotic media. As a consequence, under the nucleophilic attack of O^{2-} and Li_2O_2 to electropositive carbon, byproducts will form on graphene surface.[58,59] It is worth noting that the electropositivity of carbon in COOH and C=O is higher than that of C−O, which may lead to higher reactivity to O^{2-} and Li_2O_2. Thus, the side reaction may be suppressed by reducing the amount of oxygen and selectively removing some unstable groups.

We have also investigated the morphology of discharged electrode. As shown in Figure 7, the discharge products

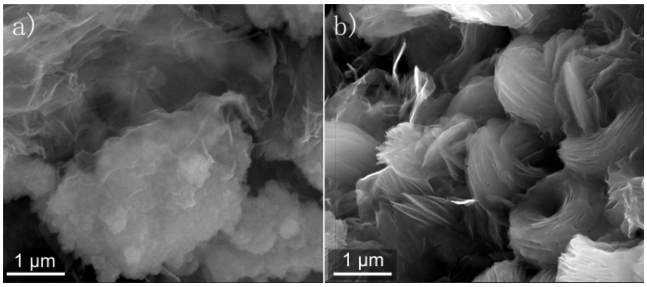

Figure 7. SEM images of (a) VTEG discharged cathode and (b) VTEG-HT discharged cathode.

distributed on VTEG surface show an amorphous morphology. Closer inspection reveals that the larger particles of 2−3 μm size are composed of nanoparticles of 70−100 nm. For VTEG-HT cathode, the solid products display perfect toroidal structure consisting of bundles of nanosheets with a thickness of 30−60 nm and up to 2 μm in length, which is consistent with literature reports.[16] The well-defined morphology on VTEG-HT cathode maybe attributed to the preferential growth of Li_2O_2 on Li_2O_2 surfaces,[30] which is expected to deliver large capacity.[60] In contrast, the growth of Li_2O_2 on VTEG surface is partially restricted by the Li_2CO_3 layer. However, it is reported that the amorphous Li_2O_2 particles with less O-rich surfaces exhibit better rechargeability than toroidal type products[30,61] due to the morphology effect. While, in fact, the cycle stability of VTEG-HT cathode is far better than that of VTEG cathode. This further confirms that the stable electrochemical reaction interface of VTEG-HT can reduce the amount of byproducts.

4. CONCLUSION

In summary, we have successfully fabricated a hierarchically structured graphene matrix with well-tuned surface chemical environment via a vacuum-promoted, thermal expansion method followed by a deoxygenation method to tailor surface oxygen groups. The unique combination of the open porous structure and deoxygenated graphene surface exhibits a high discharge capacity of 19 800 mA h g^{-1} and operates over 50 cycles at 1000 mA g^{-1}. This is mainly attributed to the synergistic effect of the hierarchical structure and the stable surface chemistry, which provides numerous reaction sites, strengthens the reactant transfer, and reduces the formation of byproducts. Our results introduce a new way to design oxygen electrode for Li−O_2 batteries with high capacity and high cycling stability.

■ ASSOCIATED CONTENT

Supporting Information

XPS survey of graphite oxide; TEM observations of CRG and VTEG; N_2 adsorption−desorption isotherms; pore parameters of CRG, VTEG, and VTEG-HT; discharge curve of CRG cathode at 1000 mA g^{-1}; thermogravimetric analysis curves; TEM and SEM microscopy of VTEG-HT; and impedance spectra. This material is available free of charge via the Internet at http://pubs.acs.org.

■ AUTHOR INFORMATION

Corresponding Authors

*E-mail: zhanghm@dicp.ac.cn.
*E-mail: zhangyn@dicp.ac.cn.

Notes

The authors declare no competing financial interest.

■ ACKNOWLEDGMENTS

The authors acknowledge financial support from National Natural Science Foundation of China (No. 51403209) and 100 Talents Program of Dalian Institute of Chemical Physics.

■ REFERENCES

(1) Bruce, P. G.; Freunberger, S. A.; Hardwick, L. J.; Tarascon, J.-M. Li−O_2 and Li−S Batteries with High Energy Storage. *Nat. Mater.* **2012**, *11*, 19−29.

(2) Jeong, G.; Kim, Y.-U.; Kim, H.; Kim, Y.-J.; Sohn, H.-J. Prospective Materials and Applications for Li Secondary Batteries. *Energy Environ. Sci.* **2011**, *4*, 1986−2002.

(3) Shao, Y.; Ding, F.; Xiao, J.; Zhang, J.; Xu, W.; Park, S.; Zhang, J.-G.; Wang, Y.; Liu, J. Making Li−Air Batteries Rechargeable: Material Challenges. *Adv. Funct. Mater.* **2013**, *23*, 987−1004.

(4) McCloskey, B. D.; Bethune, D. S.; Shelby, R. M.; Girishkumar, G.; Luntz, A. C. Solvents' Critical Role in Nonaqueous Lithium-Oxygen Battery Electrochemistry. *J. Phys. Chem. Lett.* **2011**, *2*, 1161−1166.

(5) Freunberger, S. A.; Chen, Y.; Peng, Z.; Griffin, J. M.; Hardwick, L. J.; Barde, F.; Novak, P.; Bruce, P. G. Reactions in the Rechargeable Lithium-O_2 Battery with Alkyl Carbonate Electrolytes. *J. Am. Chem. Soc.* **2011**, *133*, 8040−8047.

(6) Freunberger, S. A.; Chen, Y. H.; Drewett, N. E.; Hardwick, L. J.; Barde, F.; Bruce, P. G. The Lithium−Oxygen Battery with Ether-Based Electrolytes. *Angew. Chem., Int. Ed.* **2011**, *50*, 8609−8613.

(7) McCloskey, B. D.; Speidel, A.; Scheffler, R.; Miller, D. C.; Viswanathan, V.; Hummelshoj, J. S.; Norskov, J. K.; Luntz, A. C. Twin Problems of Interfacial Carbonate Formation in Nonaqueous Li−O_2 Batteries. *J. Phys. Chem. Lett.* **2012**, *3*, 997−1001.

DOI: 10.1021/am508513m
ACS Appl. Mater. Interfaces 2015, 7, 3389−3397

(8) Thotiyl, M. M. O.; Freunberger, S. A.; Peng, Z. Q.; Bruce, P. G. The Carbon Electrode in Nonaqueous Li–O_2 Cells. *J. Am. Chem. Soc.* **2013**, *135*, 494–500.
(9) Shao, Y. Y.; Ding, F.; Xiao, J.; Zhang, J.; Xu, W.; Park, S.; Zhang, J. G.; Wang, Y.; Liu, J. Making Li–Air Batteries Rechargeable: Material Challenges. *Adv. Funct. Mater.* **2013**, *23*, 987–1004.
(10) Xiao, J.; Mei, D.; Li, X.; Xu, W.; Wang, D.; Graff, G. L.; Bennett, W. D.; Nie, Z.; Saraf, L. V.; Aksay, I. A.; Liu, J.; Zhang, J. G. Hierarchically Porous Graphene as a Lithium–Air Battery Electrode. *Nano Lett.* **2011**, *11*, 5071–5078.
(11) Wang, Z. L.; Xu, D.; Xu, J. J.; Zhang, L. L.; Zhang, X. B. Graphene Oxide Gel-Derived, Free-Standing, Hierarchically Porous Carbon for High-Capacity and High-Rate Rechargeable Li–O_2 Batteries. *Adv. Funct. Mater.* **2012**, *22*, 3699–3705.
(12) Li, F.; Tang, D.-M.; Chen, Y.; Golberg, D.; Kitaura, H.; Zhang, T.; Yamada, A.; Zhou, H. Ru/ITO: A Carbon-Free Cathode for Nonaqueous Li–O_2 Battery. *Nano Lett.* **2013**, *13*, 4702–4707.
(13) Lim, H.-D.; Song, H.; Gwon, H.; Park, K.-Y.; Kim, J.; Bae, Y.; Kim, H.; Jung, S.-K.; Kim, T.; Kim, Y. H.; Lepró, X.; Ovalle-Robles, R.; Baughman, R. H.; Kang, K. A New Catalyst-Embedded Hierarchical Air Electrode for High-Performance Li–O_2 Batteries. *Energy Environ. Sci.* **2013**, *6*, 3570–3575.
(14) Xu, J.-J.; Wang, Z.-L.; Xu, D.; Zhang, L.-L.; Zhang, X.-B., Tailoring Deposition and Morphology of Discharge Products towards High-Rate and Long-Life Lithium–Oxygen Batteries. *Nat. Commun.* **2013**, *4*.
(15) Lu, J.; Lei, Y.; Lau, K. C.; Luo, X.; Du, P.; Wen, J.; Assary, R. S.; Das, U.; Miller, D. J.; Elam, J. W.; Albishri, H. M.; El-Hady, D. A.; Sun, Y.-K.; Curtiss, L. A.; Amine, K., A Nanostructured Cathode Architecture for Low Charge Overpotential in Lithium–Oxygen Batteries. *Nat. Commun.* **2013**, *4*.
(16) Ottakam Thotiyl, M. M.; Freunberger, S. A.; Peng, Z. Q.; Chen, Y. H.; Liu, Z.; Bruce, P. G. A Stable Cathode for the Aprotic Li–O_2 Battery. *Nat. Mater.* **2013**, *12*, 1050–1056.
(17) Peng, Z.; Freunberger, S. A.; Chen, Y.; Bruce, P. G. A Reversible and Higher-Rate Li–O_2 Battery. *Science* **2012**, *337*, 563–566.
(18) Li, J.; Zhang, H.; Zhang, Y.; Wang, M.; Zhang, F.; Nie, H. A Hierarchical Porous Electrode Using a Micron-Sized Honeycomb-like Carbon Material for High Capacity Lithium–Oxygen Batteries. *Nanoscale* **2013**, *5*, 4647–4651.
(19) Albertus, P.; Girishkumar, G.; McCloskey, B.; Sánchez-Carrera, R. S.; Kozinsky, B.; Christensen, J.; Luntz, A. C. Identifying Capacity Limitations in the Li/Oxygen Battery Using Experiments and Modeling. *J. Electrochem. Soc.* **2011**, *158*, A343–A351.
(20) Choi, N. S.; Chen, Z. H.; Freunberger, S. A.; Ji, X. L.; Sun, Y. K.; Amine, K.; Yushin, G.; Nazar, L. F.; Cho, J.; Bruce, P. G. Challenges Facing Lithium Batteries and Electrical Double-Layer Capacitors. *Angew. Chem., Int. Ed.* **2012**, *51*, 9994–10024.
(21) Zhang, Y.; Zhang, H.; Li, J.; Wang, M.; Nie, H.; Zhang, F. The Use of Mixed Carbon Materials with Improved Oxygen Transport in a Lithium–Air Battery. *J. Power Sources* **2013**, *240*, 390–396.
(22) Nie, H.; Zhang, H.; Zhang, Y.; Liu, T.; Li, J.; Lai, Q. Nitrogen Enriched Mesoporous Carbon as a High Capacity Cathode in Lithium–Oxygen Batteries. *Nanoscale* **2013**, *5*, 8484–8487.
(23) Lin, X.; Zhou, L.; Huang, T.; Yu, A. Hierarchically Porous Honeycomb-like Carbon as a Lithium–Oxygen Electrode. *J. Mater. Chem. A* **2013**, *1*, 1239–1245.
(24) Zhang, Z.; Bao, J.; He, C.; Chen, Y.; Wei, J.; Zhou, Z. Hierarchical Carbon–Nitrogen Architectures with Both Mesopores and Macrochannels as Excellent Cathodes for Rechargeable Li-O_2 Batteries. *Adv. Funct. Mater.* **2014**, *24*, 6826–6833.
(25) Lim, H.-D.; Park, K.-Y.; Song, H.; Jang, E. Y.; Gwon, H.; Kim, J.; Kim, Y. H.; Lima, M. D.; Robles, R. O.; Lepró, X.; Baughman, R. H.; Kang, K. Enhanced Power and Rechargeability of a Li–O_2 Battery Based on a Hierarchical-Fibril CNT Electrode. *Adv. Mater.* **2013**, *25*, 1348–1352.
(26) Mitchell, R. R.; Gallant, B. M.; Thompson, C. V.; Shao-Horn, Y. All-Carbon-Nanofiber Electrodes for High-Energy Rechargeable Li–O_2 Batteries. *Energy Environ. Sci.* **2011**, *4*, 2952–2958.
(27) Li, Y. L.; Wang, J. J.; Li, X. F.; Geng, D. S.; Li, R. Y.; Sun, X. L. Superior Energy Capacity of Graphene Nanosheets for a Nonaqueous Lithium–Oxygen Battery. *Chem. Commun.* **2011**, *47*, 9438–9440.
(28) Wang, J.; Li, Y.; Sun, X. Challenges and Opportunities of Nanostructured Materials for Aprotic Rechargeable Lithium–Air Batteries. *Nano Energy* **2013**, *2*, 443–467.
(29) Kraytsberg, A.; Ein-Eli, Y. The Impact of Nano-Scaled Materials on Advanced Metal–Air Battery Systems. *Nano Energy* **2013**, *2*, 468–480.
(30) Gallant, B. M.; Kwabi, D. G.; Mitchell, R. R.; Zhou, J.; Thompson, C. V.; Shao-Horn, Y. Influence of Li_2O_2 Morphology on Oxygen Reduction and Evolution Kinetics in Li–O_2 Batteries. *Energy Environ. Sci.* **2013**, *6*, 2518–2528.
(31) Zhang, Z.; Su, L.; Yang, M.; Hu, M.; Bao, J.; Wei, J.; Zhou, Z. A Composite of Co Nanoparticles Highly Dispersed on N-Rich Carbon Substrates: An Efficient Electrocatalyst for Li–O_2 Battery Cathodes. *Chem. Commun.* **2014**, *50*, 776–778.
(32) Sun, B.; Munroe, P.; Wang, G., Ruthenium Nanocrystals as Cathode Catalysts for Lithium–Oxygen Batteries with a Superior Performance. *Sci. Rep.* **2013**, *3*.
(33) Choi, R.; Jung, J.; Kim, G.; Song, K.; Kim, Y.-I.; Jung, S. C.; Han, Y.-K.; Song, H.; Kang, Y.-M. Ultra-Low Overpotential and High Rate Capability in Li–O_2 Batteries through Surface Atom Arrangement of PdCu Nanocatalysts. *Energy Environ. Sci.* **2014**, *7*, 1362–1368.
(34) Black, R.; Lee, J. H.; Adams, B.; Mims, C. A.; Nazar, L. F. The Role of Catalysts and Peroxide Oxidation in Lithium–Oxygen Batteries. *Angew. Chem., Int. Ed.* **2013**, *52*, 392–396.
(35) Jian, Z.; Liu, P.; Li, F.; He, P.; Guo, X.; Chen, M.; Zhou, H. Core-Shell-Structured CNT@RuO_2 Composite as a High-Performance Cathode Catalyst for Rechargeable Li–O_2 Batteries. *Angew. Chem., Int. Ed.* **2014**, *53*, 442–446.
(36) Zhou, W.; Li, J.; Nie, H.; Zhang, Y.; Xi, X.; Zhang, H. Carbon Electrode for Nonaqueous Li–O_2 Battery: The Influence of Surface Oxygen Species. *Electrochim. Acta* **2014**, *138*, 410–416.
(37) Itkis, D. M.; Semenenko, D. A.; Kataev, E. Y.; Belova, A. I.; Neudachina, V. S.; Sirotina, A. P.; Hävecker, M.; Teschner, D.; Knop-Gericke, A.; Dudin, P.; Barinov, A.; Goodilin, E. A.; Shao-Horn, Y.; Yashina, L. V. Reactivity of Carbon in Lithium–Oxygen Battery Positive Electrodes. *Nano Lett.* **2013**, *13*, 4697–4701.
(38) Chen, C.-M.; Zhang, Q.; Huang, C.-H.; Zhao, X.-C.; Zhang, B.-S.; Kong, Q.-Q.; Wang, M.-Z.; Yang, Y.-G.; Cai, R.; Sheng, S. D. Macroporous "Bubble" Graphene Film via Template-Directed Ordered-Assembly for High Rate Supercapacitors. *Chem. Commun.* **2012**, *48*, 7149.
(39) Stankovich, S.; Dikin, D. A.; Dommett, G. H. B.; Kohlhaas, K. M.; Zimney, E. J.; Stach, E. A.; Piner, R. D.; Nguyen, S. T.; Ruoff, R. S. Graphene-based Composite Materials. *Nature* **2006**, *442*, 282–286.
(40) Sun, B.; Wang, B.; Su, D.; Xiao, L.; Ahn, H.; Wang, G. Graphene Nanosheets as Cathode Catalysts for Lithium–Air Batteries with an Enhanced Electrochemical Performance. *Carbon* **2012**, *50*, 727–733.
(41) Stankovich, S.; Dikin, D. A.; Piner, R. D.; Kohlhaas, K. A.; Kleinhammes, A.; Jia, Y.; Wu, Y.; Nguyen, S. T.; Ruoff, R. S. Synthesis of Graphene-based Nanosheets via Chemical Reduction of Exfoliated Eraphite Oxide. *Carbon* **2007**, *45*, 1558–1565.
(42) Marcano, D. C.; Kosynkin, D. V.; Berlin, J. M.; Sinitskii, A.; Sun, Z.; Slesarev, A.; Alemany, L. B.; Lu, W.; Tour, J. M. Improved Synthesis of Graphene Oxide. *ACS Nano* **2010**, *4*, 4806–4814.
(43) Li, D.; Muller, M. B.; Gilje, S.; Kaner, R. B.; Wallace, G. G. Processable Aqueous Dispersions of Graphene Nanosheets. *Nat. Nanotechnol.* **2008**, *3*, 101–105.
(44) Lv, W.; Tang, D.-M.; He, Y.-B.; You, C.-H.; Shi, Z.-Q.; Chen, X.-C.; Chen, C.-M.; Hou, P.-X.; Liu, C.; Yang, Q.-H. Low-Temperature Exfoliated Graphenes: Vacuum-Promoted Exfoliation and Electrochemical Energy Storage. *ACS Nano* **2009**, *3*, 3730–3736.
(45) Byon, H. R.; Gallant, B. M.; Lee, S. W.; Shao-Horn, Y. Role of Oxygen Functional Groups in Carbon Nanotube/Graphene Free-standing Electrodes for High Performance Lithium Batteries. *Adv. Funct. Mater.* **2013**, *23*, 1037–1045.

DOI: 10.1021/am508513m
ACS Appl. Mater. Interfaces 2015, 7, 3389–3397

(46) Achour, A.; Vizireanu, S.; Dinescu, G.; Le Brizoual, L.; Djouadi, M. A.; Boujtita, M. Electrochemical Anodic Oxidation of Nitrogen Doped Carbon Nanowall Films: X-ray Photoelectron and Micro-Raman Spectroscopy Study. *Appl. Surf. Sci.* **2013**, *273*, 49−57.
(47) Arrigo, R.; Hävecker, M.; Wrabetz, S.; Blume, R.; Lerch, M.; McGregor, J.; Parrott, E. P.; Zeitler, J. A.; Gladden, L. F.; Knop-Gericke, A. Tuning the Acid/Base Properties of Nanocarbons by Functionalization via Amination. *J. Am. Chem. Soc.* **2010**, *132*, 9616−9630.
(48) Chen, C.-M.; Zhang, Q.; Zhao, X.-C.; Zhang, B.; Kong, Q.-Q.; Yang, M.-G.; Yang, Q.-H.; Wang, M.-Z.; Yang, Y.-G.; Schlögl, R.; Su, D. S. Hierarchically Aminated Graphene Honeycombs for Electrochemical Capacitive Energy Storage. *J. Mater. Chem.* **2012**, *22*, 14076.
(49) Chen, C.-M.; Zhang, Q.; Yang, M.-G.; Huang, C.-H.; Yang, Y.-G.; Wang, M.-Z. Structural Evolution During Annealing of Thermally Reduced Graphene Nanosheets for Application in Supercapacitors. *Carbon* **2012**, *50*, 3572−3584.
(50) Yang, D.; Velamakanni, A.; Bozoklu, G.; Park, S.; Stoller, M.; Piner, R. D.; Stankovich, S.; Jung, I.; Field, D. A.; Ventrice, C. A.; Ruoff, R. S. Chemical Analysis of Graphene Oxide Films after Heat and Chemical Treatments by X-ray Photoelectron and Micro-Raman Spectroscopy. *Carbon* **2009**, *47*, 145−152.
(51) Jabari Seresht, R.; Jahanshahi, M.; Rashidi, A.; Ghoreyshi, A. A. Synthesize and Characterization of Graphene Nanosheets with High Surface Area and Nano-porous Structure. *Appl. Surf. Sci.* **2013**, *276*, 672−681.
(52) Gierszal, K. P.; Jaroniec, M.; Kim, T.-W.; Kim, J.; Ryoo, R. High Temperature Treatment of Ordered Mesoporous Carbons Prepared by Using Various Carbon Precursors and Ordered Mesoporous Silica Templates. *New J. Chem.* **2008**, *32*, 981.
(53) Mirzaeian, M.; Hall, P. J. Characterizing Capacity Loss of Lithium Oxygen Batteries by Impedance Spectroscopy. *J. Power Sources* **2010**, *195*, 6817−6824.
(54) Nelson, R.; Weatherspoon, M. H.; Gomez, J.; Kalu, E. E.; Zheng, J. P. Investigation of a Li−O_2 Cell Featuring a Binder-free Cathode via Impedance Spectroscopy and Equivalent Circuit Model Analysis. *Electrochem. Commun.* **2013**, *34*, 77−80.
(55) Kim, B. G.; Lee, J.-N.; Lee, D. J.; Park, J.-K.; Choi, J. W. Robust Cycling of Li-O_2 Batteries through the Synergistic Effect of Blended Electrolytes. *ChemSusChem* **2013**, *6*, 443−448.
(56) Lu, Y.-C.; Crumlin, E. J.; Veith, G. M.; Harding, J. R.; Mutoro, E.; Baggetto, L.; Dudney, N. J.; Liu, Z.; Shao-Horn, Y., In Situ Ambient Pressure X-ray Photoelectron Spectroscopy Studies of Lithium−Oxygen Redox Reactions. *Sci. Rep.* **2012**, *2*.
(57) Sawyer, D. T.; Valentine, J. S. How Super Is Superoxide? *Acc. Chem. Res.* **1981**, *14*, 393−400.
(58) Gibian, M. J.; Sawyer, D. T.; Ungermann, T.; Tangpoonpholvivat, R.; Morrison, M. M. Reactivity of Superoxide Ion with Carbonyl Compounds in Aprotic Solvents. *J. Am. Chem. Soc.* **1979**, *31*, 640−644.
(59) Bryantsev, V. S.; Blanco, M. Computational Study of the Mechanisms of Superoxide-Induced Decomposition of Organic Carbonate-Based Electrolytes. *J. Phys. Chem. Lett.* **2011**, *2*, 379−383.
(60) Aetukuri, N. B.; McCloskey, B. D.; García, J. M.; Krupp, L. E.; Viswanathan, V.; Luntz, A. C. Solvating Additives Drive Solution-Mediated Electrochemistry and Enhance Toroid Growth in Non-Aqueous Li−O_2 Batteries. *Nat. Chem.* **2014**, *7*, 50−56.
(61) Adams, B. D.; Radtke, C.; Black, R.; Trudeau, M. L.; Zaghib, K.; Nazar, L. F. Current Density Dependence of Peroxide Formation in the Li−O_2 Battery and Its Effect on Charge. *Energy Environ. Sci.* **2013**, *6*, 1772−1778.

DOI: 10.1021/am508513m
ACS Appl. Mater. Interfaces 2015, 7, 3389−3397